TEKTONIKA

Inverted Magma-rich Versus Magma-poor Rifted Margins: Implications for Early Orogenic Systems

Júlia Gómez-Romeu *[1], **Suzon Jammes** [1], **Maxime Ducoux** [1], **Rodolphe Lescoutre** [1], **Sylvain Calassou** [2], **Emmanuel Masini** [1,3]

[1]M&U sas, Sassenage, France | [2]Total R&D, Pau, France | [3]ISTerre, Earth Sciences Institute, Grenoble, France

Abstract Mountain belts are often the result of former inverted rifts or rifted margins. Up to date, relics of magma-poor rifted margins have been found in orogens allowing the investigation of how these margins reactivate and control the formation of mountain belts. In contrast, magma-rich rifted margins have barely been recognized within orogenic systems, and consequently how these margins reactivate and control subsequent orogenesis is poorly understood. We use a thermo-mechanical model to investigate the mechanical behaviour of reactivated magma-rich versus magma-poor rifted margins during early orogenesis (i.e. margin inversion). Input data for our modelling experiments are obtained from two natural laboratories. One is the Demerara Plateau characterized by a mildly shortened magma-rich rifted margin. Its décollement level is observed at the top of the syn-kinematic volcanics, which propagates downwards into a frozen incipient subduction. The other study-case is the Basque-Cantabrian Belt consisting of a reactivated magma-poor hyper-extended rift system with the décollement level at the bottom of the syn-rift sediments. Our modelling results, for inverted magma-rich rifted margin, show that the syn-kinematic volcanics undergo subduction as they are mechanically coupled with the underlying rifted lithosphere. Hence, only post-rift sediments are accreted within the early orogenic accretionary wedge. In contrast, both the syn- and post-rift sediments from a reactivated magma-poor rifted margin are expected to be preserved within the accretionary wedge. Therefore, we conclude that the presence or absence of syn-rift sediments within an accretionary prism may represent a robust indicator to determine the nature of reactivated rifted margins within orogens. We believe that our results may strongly contribute to recognize, the so far poorly identified, magma-rich rifted margins within present-day orogenic systems.

Executive Editor:
Janine Kavanagh
Associate Editor:
Adam Forte
Technical Editor:
Mohamed Gouiza

Reviewers:
Frank Zwaan
Anouk Beniest

Submitted:
28 July 2022
Accepted:
9 February 2023
Published:
20 March 2023

1 Introduction

Passive margins are extensively distributed worldwide and can be classified as magma-poor, magma-rich or transform (Figure 1). Almost half of the worldwide rifted margins are magma-rich (Figures 1a and 1c). However only a very few relics of magma-rich rifted margins within Paleozoic orogens have so far been reported (in the Caledonides mountains as shown by *Jakob et al.* (2019, 2022)). A key question is why magma-rich rifted margins have not been found within Meso-Cenozoic orogens, while the magma-poor end-member is well recognized? Are all magma-rich rifted margins fully subducted and thus their initial record cannot be found in orogens, or have they not been identified yet?

Due to an increase of offshore seismic reflection data acquisition, mostly by industry, magma-poor rifted margins have been extensively studied for the last three decades (Figure 1a and 1b). This has allowed to define their crustal and basin architecture, the stratigraphic record, key structural domains, and thus better understand their formation (e.g. *Davis and Kusznir*, 2004; *Kusznir and Karner*, 2007; *Péron-Pinvidic and Manatschal*, 2009; *Mohn et al.*, 2010; *Ranero and Pérez-Gussinyé*, 2010; *Osmundsen and Redfield*, 2011; *Sutra and Manatschal*, 2012; *Huismans and Beaumont*, 2014; *Tugend et al.*, 2014; *Jeanniot et al.*, 2016; *Gillard et al.*, 2017; *Nirrengarten et al.*, 2017). The recognition of deformed magma-poor rifted margins relics accreted within mountain belts such as in the Alps (e.g. *Lemoine et al.*, 1987; *Manatschal*, 2004; *Mohn et al.*, 2010; *Beltrando et al.*, 2014; *Manatschal et al.*, 2022; *Chenin et al.*, 2022) and in the Pyrenees (e.g. *Jammes et al.*, 2009; *Masini et al.*, 2014; *Tugend et al.*, 2014; *Jourdon et al.*, 2019; *Lagabrielle et al.*, 2020; *Lescoutre and Manatschal*, 2020; *Saspiturry et al.*, 2020; *Ducoux et al.*, 2021), has allowed the interplay between rift inheritance and plate convergence from subduction to continent-continent collision to be investigated. The pre-orogenic rift template of the Pyrenees and the western Alps consists of a magma-poor rift system (Figure 1b) that evolved up to the formation of the exhumed subcontinental mantle (i.e. an ocean-continent transition) and a narrow oceanic domain, respectively (*Jammes et al.*, 2009; *Masini et al.*, 2014; *Mohn et al.*, 2010; *Chenin et al.*, 2017). Despite this different divergence maturity between the Pyrenees

*✉ julia@mandu-geology.fr

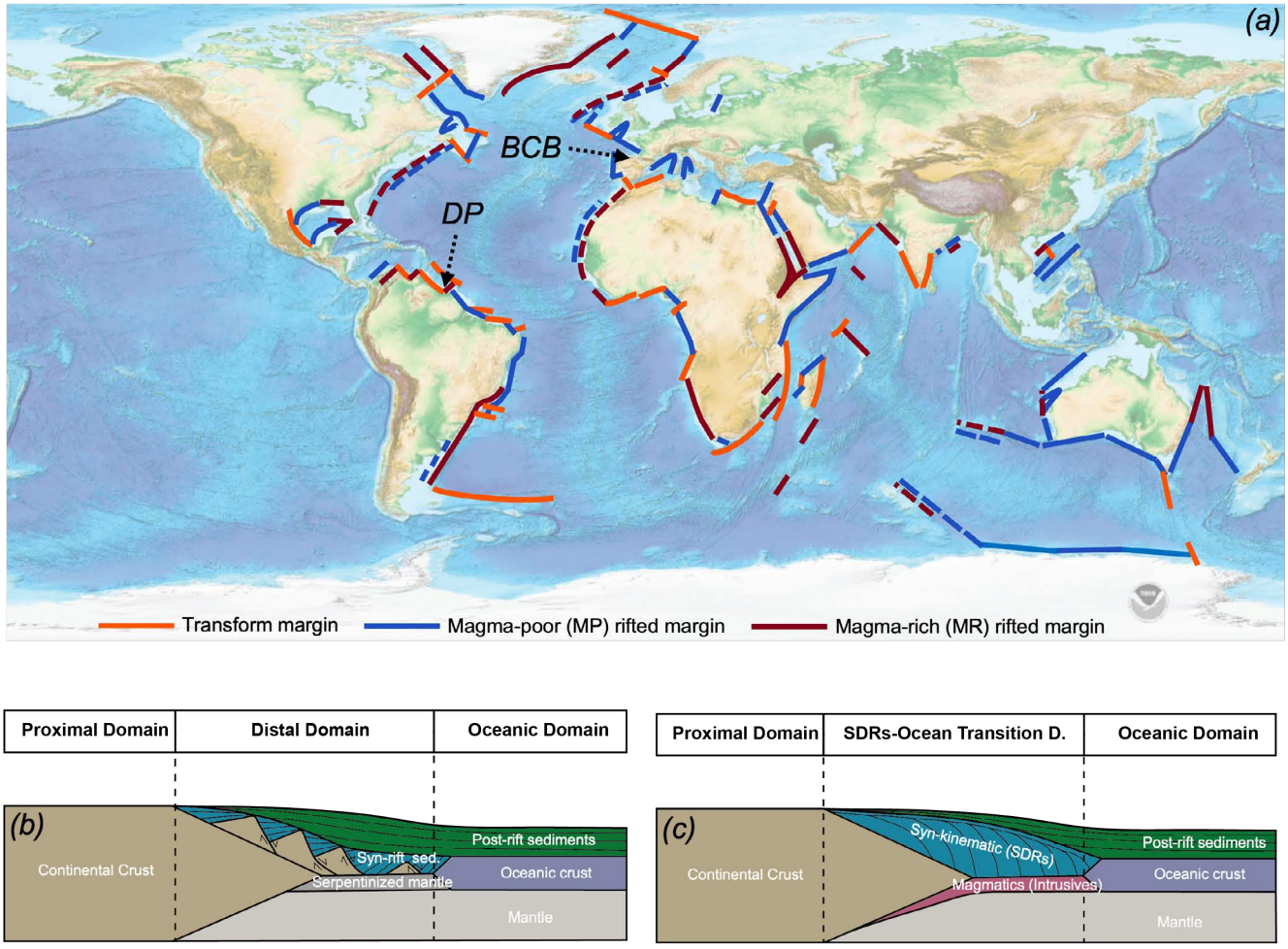

Figure 1 – **a)** Bathymetric global map showing the different types of passive margins worldwide (modified after *Haupert et al.* (2016) who used the map from the National Geophysical Data Centre). DP: Demerara Plateau, BCB: Basque-Cantabrian Belt. **b-c)** A schematic magma-poor and magma-rich rifted margins respectively. SDRs: Seaward Dipping Reflectors; D: Domain.

and the Alps, it has been shown that the present-day orogenic architecture resulted from the sequential reactivation of pre-existing rift domains for both cases, from distal to proximal (e.g. *Mohn et al.*, 2010, 2012; *Tugend et al.*, 2014; *Masini et al.*, 2014; *Gómez-Romeu et al.*, 2019; *Tavani et al.*, 2021), and consequently that rift inheritance strongly controlled the formation of these orogens.

Rifted margins can also be magma-rich when associated with significant amounts of magmatic additions during their formation, modifying crustal thickness, its composition and obscuring tectonic structures (Figure 1c). Some studies, mostly based on seismic reflection, refraction and radiometric data, have shown the architecture of magma-rich rifted margins and proposed conceptual models to explain their formation (*Shillington et al.*, 2009; *Stica et al.*, 2014; *Reuber et al.*, 2016; *Stab et al.*, 2016; *Norcliffe et al.*, 2018; *Lundin et al.*, 2018; *Kjøll et al.*, 2019; *Gouiza and Paton*, 2019; *Tugend et al.*, 2020; *Tomasi et al.*, 2021; *Watremez et al.*, 2021; *Gómez-Romeu et al.*, 2022). The architecture of magma-rich rifted margins stands out by the presence of Seaward Dipping Reflectors (SDRs) on top of intrusive and underplated magmatics in the distal part of the margin (Figure 1c). In contrast, its distal magma-poor end-member margin is characterized by extensional fault blocks on top of hyper-thinned continental crust and serpentinized exhumed mantle (e.g. *Sutra et al.*, 2013) (Figure 1b). A recent study, using a numerical modelling approach, reported how magma-rich rifted margins interact with the onset of subduction and suggested that subduction initiates within the oceanic lithosphere (*Auzemery et al.*, 2022). Nevertheless, still many questions remain, such as, how do inverted magma-rich rifted margins evolve during a more mature collisional stage and lead to the formation of orogens?

To address this question, a better understanding of the mechanical behaviour of reactivated magma-rich rifted margins during orogenesis, from subduction initiation until eventual orogen formation, is needed. We believe that better understanding how magma-rich and magma-poor rifted margins reactivate may provide insights on identifying relics of magma-rich rifted margins within present-day orogens worldwide.

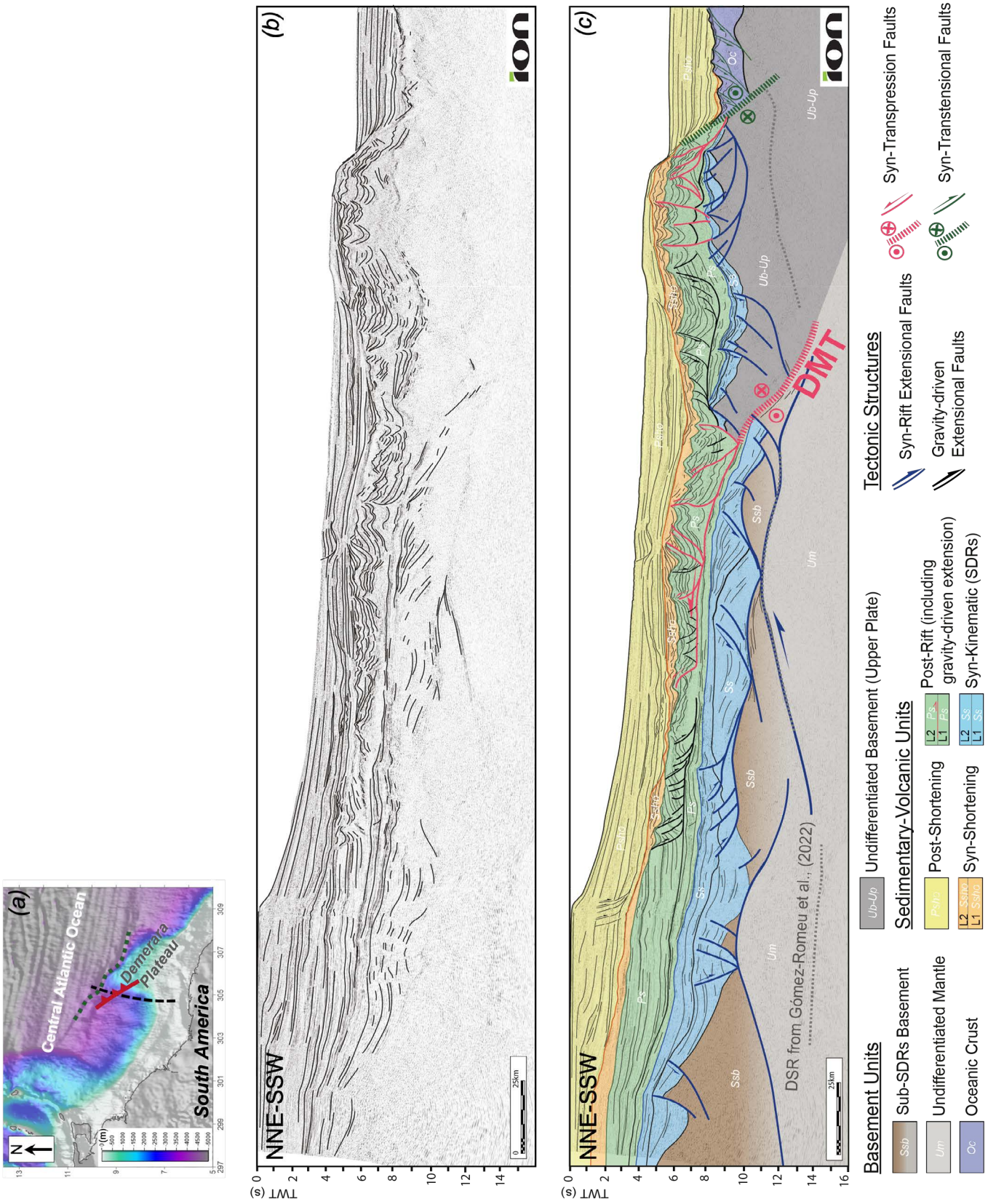

Figure 2 – **a)** Bathymetry and free-air shaded relief map of the southern Central Atlantic Ocean, Demerara Plateau and northern Equatorial Atlantic Ocean (modified after *Gómez-Romeu et al.*, 2022). The black dashed line shows the position of the seismic profile used in b and c. **b-c)** Line-drawing of an ION seismic profile and its interpretation in **c)**. DMT: Demerara Main Thrust. In **c)** thick red line: tickskin deformation, thin red line: thin-skin deformation.

2 Research Strategy

The research strategy of this study consists of using a thermo-mechanical modelling approach to investigate how magma-rich and magma-poor rifted margins reactivate during early orogenesis. In particular, we investigate the mechanical behaviour of these two end-member rifted margins during early orogenesis, or immature collision (*Gómez-Romeu et al.*, 2019), which results from the inversion of distal rifted margins that are nowadays preserved in orogenic systems. To achieve our research aim, we use two natural laboratories that underwent first rifting and then early orogenesis. They consist of the offshore western Demerara Plateau, located in eastern South America, and the onshore Basque-Cantabrian Belt in northern Iberia (Figure 1a). The former is characterized by a mildly shortened distal magma-rich rifted margin (Figure 2) while the latter is characterized by a reactivated magma-poor hyper-extended rift system (Figure 3). The analysis of seismic data of the western Demerara Plateau and the Basque-Cantabrian Belt allows us to determine key observations such as the location of the main convergence décollement level. Determining this allows us to distinguish between the subducted units from those accreted in the accretionary wedge and thus gain insights on how rifted margins deform under shortening. Our modelling strategy consists of using large-scale present-day observations from our case studies to constrain our modelling experiments. The modelling input data corresponds to the pre-orogenic rifted margin architecture and the location of the convergence décollement level. Note that we do not aim to reproduce the detailed geology of the western Demerara Plateau nor the Basque-Cantabrian Belt. Through this modelling approach we determine (i) how the position of the convergence décollement level evolves through early orogenesis and (ii) the units preserved in the early orogenic wedge and those that subduct. The exploration of late orogenesis, or mature collision, consisting of shortened proximal rift domain leading to crustal thickening (*Gómez-Romeu et al.*, 2019) is out of the scope of this study.

3 Geological Setting and Orogenic Architecture of Two Natural Laboratories

A brief geological setting of both study-cases is given below, followed by key orogenic observations obtained from literature and based on our own assessment.

3.1 Magma-rich Rifted Margin: the Western Demerara Plateau Example

3.1.1 Geological Setting

The Demerara Plateau is characterized by a western Jurassic magma-rich rifted segment, formed during the opening of the Central Atlantic Ocean, and a northern transform margin juxtaposing Jurassic Central Atlantic with Cretaceous Equatorial Atlantic oceanic crusts (Figure 1) (*Gouyet et al.*, 1994; *Greenroyd et al.*, 2007; *Basile et al.*, 2013; *Nemčok et al.*, 2016; *Mercier de Lépinay et al.*, 2016; *Loncke et al.*, 2022; *Loparev et al.*, 2021). Crustal-scale shortening offshore the Demerara Plateau has been reported by *Museur et al.* (2021); *Loparev et al.* (2021); *Trude et al.* (2023), among others. This event occurred in late Lower Cretaceous, and it was suggested to result from the anticlockwise rotation of Africa with respect to South America (*Trude et al.*, 2023). This compressional event is recorded and shown in Figure 2b and 2c where well-preserved and mildly shortening features are observed, involving former distal magma-rich rifted domains (including SDRs and the Jurassic OCT, see details in *Gómez-Romeu et al.*, 2022). This shortening stopped before reaching a mature subduction in the Demerara Plateau (this is further argued in Section 4), in contrast with the neighboring Caribbean subduction further north. Based on this, we believe that the western Demerara Plateau is key to study how magma-rich rifted domains interact with early orogenesis.

3.1.2 Orogenic Architecture

The observed shortening in the Demerara Plateau (Figure 2b and 2c) is achieved by a crustal-scale thrust (i.e. thick-skin deformation), defined here as the Demerara Main Thrust (DMT). This structure leads into an under-thrusted footwall block made of basement and overlain by syn-kinematic deposits consisting of SDRs. Here we distinguish between a sub-SDRs basement, the nature of which is not addressed, from an undifferentiated mantle below (for a detailed discussion of the Demerara basement composition see *Basile et al.*, 2020; *Museur et al.*, 2021; *Gómez-Romeu et al.*, 2022) (Figure 2b and 2c).

On top of the SDRs, a post-rift unit consisting of a bottom sub-horizontal layer and an upper layer characterized by gravity-driven extensional deformation can be distinguished (Figure 2b and 2c). This deformed layer and the syn-shortening sediments above are affected by contractional structures that detach into a basal décollement level (Figure 2b and 2c). We interpret this structure as the bottom bound of thin-skinned orogenic deformation, that gives place to the early accretionary prism consisting of post-rift sediments (Figure 2b and 2c). In the profile used, the syn-kinematic SDRs are unfolded and attached to its underlying basement, both corresponding to the DMT lower plate (Figure 2b and 2c). This implies that, across the seismic profile shown in Figure 2, the syn-kinematic SDRs are mechanically coupled with the basement and mechanically decoupled from the overlying post-rift sequence, allowing for their subduction below the DMT hanging-wall. The DMT upper plate is considered here as an undifferentiated basement block overlain by thin SDRs but thick post-rift sediments (Figure 2b and 2c). Distally, the DMT upper plate is crosscut by a Cretaceous trans-

form fault bounding Cretaceous Equatorial oceanic crust.

3.2 Magma-poor Rifted Margin: the Basque-Cantabrian Belt Example

3.2.1 Geological Setting

The northern Iberian rifted margin of the Bay of Biscay is characterized by several Late Jurassic to Early Cretaceous magma-poor rift basins, such as the Basque-Cantabrian Basin which is today inverted within the Basque Cantabrian Belt (BCB) (Figure 3). These rift basins are related to the Late Jurassic to Cretaceous polyphase opening of the Southern North Atlantic Ocean and the relative motion between Iberia/Ebro and Europe (*Olivet*, 1996; *Srivastava et al.*, 1990; *Roest and Srivastava*, 1991; *Sibuet et al.*, 2004; *Macchiavelli et al.*, 2017; *Barnett-Moore et al.*, 2018). Firstly, a Late Jurassic to Early Cretaceous left-lateral transtensional rifting phase took place, followed by a a roughly NNE-SSW oriented hyper-extension rifting phase that led to mantle exhumation, while breakup and seafloor spreading occurred further NW in the Bay of Biscay (*Verhoef and Srivastava*, 1989; *Whitmarsh et al.*, 1990; *Vissers and Meijer*, 2012; *Vissers et al.*, 2016; *Tugend et al.*, 2014; *Cadenas et al.*, 2020; *Pedrera et al.*, 2017; *Tavani et al.*, 2018; *Miró et al.*, 2021). From the Late Cretaceous to Cenozoic, N-S convergence between Iberia and Europe occurred (*Macchiavelli et al.*, 2017), leading to the inversion of the hyper-extended rift to form the present-day BCB (e.g. *Pedreira et al.*, 2007; *Roca et al.*, 2011; *Pedrera et al.*, 2017; *DeFelipe et al.*, 2019; *Ducoux et al.*, 2019; *Lescoutre et al.*, 2021). No major crustal thickening related to crustal nappe-stacking is observed in the BCB, which indicates that mature continent-continent collision was not recorded. A key feature of the BCB is that most of the rift architecture remains preserved, as shown by *Lescoutre and Manatschal* (2020) and *Miró et al.* (2021). This is due to the low-orogenic maturity, in addition to the occurrence of a pre-rift salt layer that acted as a very efficient décollement level during both the rifting and orogenic stages. It triggered strain localization along the décollement, with limited brittle faulting of the Basque-Cantabrian Basin strata located above (*Ducoux et al.*, 2019; *Labaume and Teixell*, 2020; *Izquierdo-Llavall et al.*, 2020; *Cámara*, 2020). These features make the BCB a good natural laboratory to investigate the interaction between a magma-poor hyper-extended rift basin with early orogenesis.

3.2.2 Orogenic Architecture

Different tectono-sedimentary units are identified in the BCB, as defined by *Bodego et al.* (2015); *Pedrera et al.* (2017); *Martín-Chivelet et al.* (2019); *Ducoux et al.* (2019); *Lescoutre et al.* (2021), among others. For this study, we only distinguish three sedimentary units, consisting of (1) merged pre- and syn-rift (from Upper Triassic to Cenomanian), (2) post-rift (Turonian to Santonian), and (3) syn-shortening sediments (post-Santonian). The lowermost pre-rift sediments (Middle Triassic and older) are considered as undifferentiated basement as they are mechanically coupled with it (Figure 3). The distinction between the upper and lower pre-rift sediments is due to the presence of a pre-rift salt layer (*Ducoux et al.*, 2019; *Labaume and Teixell*, 2020; *Izquierdo-Llavall et al.*, 2020; *Cámara*, 2020; *Ducoux et al.*, 2021).

Tugend et al. (2014) investigated how the Basque-Cantabrian rift system reactivated under compressional tectonics, suggesting that the initiation of convergence nucleated within the serpentinized exhumed mantle, as previously proposed by *Péron-Pinvidic et al.* (2008) and *Lundin and Doré* (2011) for other rift settings. Field observations, seismic interpretation and cross-section construction of the BCB (Figure 3) show a present-day continental subduction fault plane that accommodates the underthrusting of the Iberian thinned basement. This fault plane propagates upwards as a décollement at the near basement/syn-rift sedimentary cover interface, here corresponding to the Upper Triassic evaporites, during orogenesis (see details in *Lescoutre et al.*, 2021). Consequently, most of the pre- to syn-rift sedimentary units are sampled and accreted within the early orogenic accretionary wedge through thin-skinned tectonics. Thrusted sediments are located on top of the lower plate while back-thrusted sediments are above the undifferentiated upper plate basement (Figure 3e).

4 Particularities and Strengths of our Case Studies

The local plate kinematic setting that both case studies underwent, and the justification of why they are good natural laboratories to study the reactivation of magma-rich and magma-poor rifted margins during early orogenesis, is described below.

4.1 The Western Demerara Plateau

Shortening in the Demerara Plateau (DMT) occurred due to a change of plate kinematics, characterized by the anticlockwise rotation of Africa in respect to South America (*Trude et al.*, 2023). Note that shortening in the Demerara Plateau took place simultaneously with the onset of the Caribbean mature subduction in the north. The orientation of the DMT (Figure 2) is the same as the regional Jurassic transform that occurred due to the NNW-SSE kinematic event (*Trude et al.*, 2023). Based on this, we propose that the DMT resulted from a reactivated Jurassic transform structure, leading to a forced incipient and failed mature subduction. Subduction initiation at former fracture zones, where flooding of oceanic plates by melt is likely, was already proposed by *Hynes* (2005) and *Zhou et al.* (2018).

4.2 The Basque-Cantabrian Belt

Convergence between Iberia and Europe, from east to west, led to continent-continent collision in the

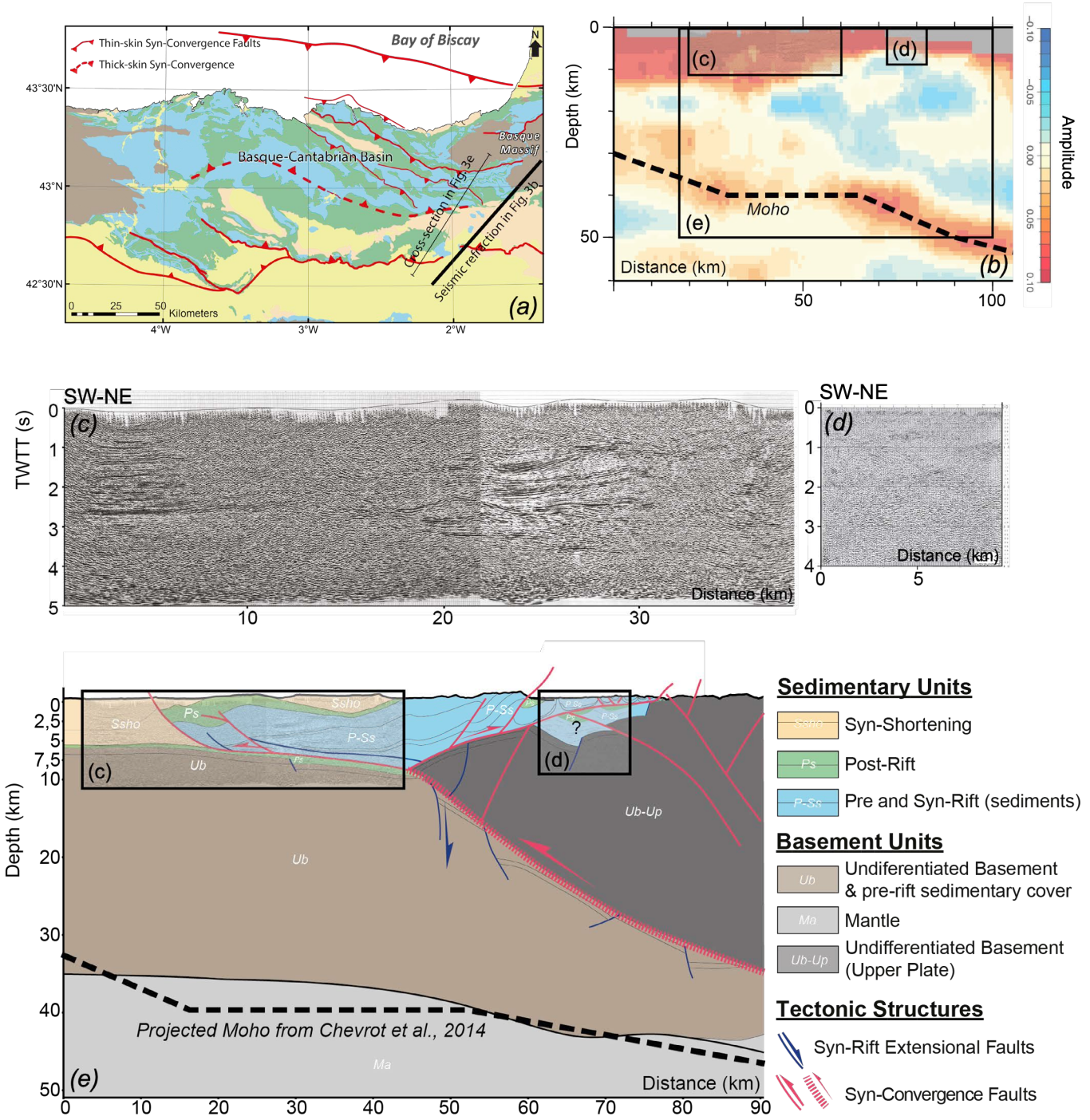

Figure 3 – a) Geological map of the Basque-Cantabrian Belt (BCB) (modified after *Ducoux et al.*, 2019). **b)** Refraction seismic profile from *Chevrot et al.* (2015) showing the deep architecture of the western Pyrenees. **c-d)** Seismic reflection profiles across the BCB from the Spanish geological survey IGME site (see their interpretation in *Lescoutre et al.*, 2021). **e)** Geological cross-section across the BCB based on field observations, reflection and refraction seismic profiles modified after *Lescoutre et al.* (2021). In **e)** thick red line: tick-skin deformation, thin red line: thin-skin deformation.

Pyrenees, early orogenesis characterized by the inversion of the hyper-extended Basque-Cantabrian basin in the BCB, and immature subduction in the Bay of Biscay (*Pedreira et al.*, 2007; *Roca et al.*, 2011; *Tugend et al.*, 2014; *Macchiavelli et al.*, 2017; *Pedrera et al.*, 2017; *DeFelipe et al.*, 2019; *Ducoux et al.*, 2019). A low-orogenic maturity system recorded in the BCB is likely due to the presence of a wider hyper-extended rift basin, this is in comparison with the neighboring Pyrenees, which is characterized by a narrower hyper-extended rift basin, and thus is a more mature orogenic system (*Masini et al.*, 2014; *Lescoutre et al.*, 2021). To achieve continent-continent collision in the BCB, as occurred in the Pyrenees, additional convergence would have been needed (*Lescoutre et al.*, 2021).

The shortening in the western Demerara Plateau and Basque-Cantabrian Belt froze at the margin inversion stage (Figures 2 and 3). Therefore, neither mature subduction nor a mature collision was developed, which favors the preservation of the early

orogenic and previous rift record in both case studies. The driving mechanism that prevented the development of a mature subduction and continent-continent collision is likely due to the plate convergence stopping too early.

5 Numerical Modelling Method and Experiments Setup

We carried out forward thermo-mechanical models to investigate the mechanical behaviour of inverted magma-rich and magma-poor rifted margins during early orogenesis. The model experiments were performed with an extended version of the numerical code PARAVOZ for Elasto-Visco-Plastic material called geoFLAC (Fast Lagrangian Analysis of Continua) (*Poliakov et al.*, 1993; *Tan et al.*, 2012; *Svartman Dias et al.*, 2015). The properties of the materials used to set up the models are given in Table 1. The aim of our modelling approach consists of determining; (i) how the location of the convergence décollement level evolves through early orogenesis, and (ii) the resulting sedimentary record of the early orogenic wedge and the subducted units.

5.1 Numerical Method

The thermo-mechanical experiments shown in Figures 4 and 5 were performed with an extended version of the numerical code PARAVOZ for Elasto-Visco-Plastic material, called geoFLAC (Fast Lagrangian Analysis of Continua) (*Poliakov et al.*, 1993; *Tan et al.*, 2012; *Svartman Dias et al.*, 2015). It is a free-access code and can be download at https://github.com/-tan2/geoflac.

At low temperatures, all materials follow Coulomb elastic plastic rheology (*Choi et al.*, 2013) as follows:

$$\tau = C + \tan(\varphi)\sigma^n$$

where τ is the shear stress at yield, C the cohesion, φ the friction angle, and σ^n the normal stress. When temperatures are high enough to activate dislocation creep, materials deform by Maxwell viscoelastic thermally activated creep. This is approximated as a non-linear temperature and strain rate dependent flow low (*Choi et al.*, 2013; *Svartman Dias et al.*, 2015). In this case, the viscosity η is calculated as:

$$\eta = \frac{1}{4}\left(\frac{4}{3A}\right)^{\frac{1}{n}} \dot{\epsilon}_{II}^{\frac{1-n}{n}} \exp\left(\frac{E}{nR(T+273)}\right)$$

where ϵ_{II} is the second invariant of the strain rate, n the stress exponent, A the viscosity pre-exponent, E the activation energy, R is the universal gas constant and T the temperature in Celsius. n, A and E are viscosity parameters from laboratory experiments. These different deformation mechanisms occur as a function of energy or effective stress (square root of the second invariant of the stress tensor). The deformation mechanism that requires less energy or effective stress is favored. The PARAVOZ code incorporates the sediment-schist metamorphic process and the mantle olivine-serpentinite hydration-dehydration process which fits for subduction modelling (*Tan et al.*, 2012; *Tan*, 2017).

The model setup of our experiments (Figures 4 and 5) is 320 km deep, 960 km long and composed of 74 by 448 elements with the finest grid (3x1.5 km) located in the middle (between 300 and 660 km) up to 50 km depth. Velocity boundary conditions are imposed on the left side of the models (velocity = 5 cm.yr^{-1}, in compression following *Tan et al.* (2012) and *Tan* (2017). To allow for topographic build-up of the lithosphere, the top surface of the lithosphere is treated as an internal free surface by using a top layer (of 20 km thickness) with low viscosity (1018 Pa.s) and low density (1 kg.m^{-3} for air). A Winkler foundation is imposed at the base of the model to maintain isostatic equilibrium. The crust is 30 km thick in the proximal domain, but towards the distal domain it gradually decreases to 0 km which leads to a taper geometry typical of rifted margins. The initial temperature is set up at 10°C at the surface of the continental plate and at 550°C at the continental crust- mantle boundary while it increases up to 1330°C at 100 km depth. Strain softening is introduced in the models by a linear decrease of cohesion and friction angle to account for the formation of faults. It occurs when the plastic strain is higher than 0.1 with a loss of cohesion from C = 40 MPa to C = 4 MPa and a change of friction angle from ϕ=30°C to ϕ=15°C (*Lavier et al.*, 2000; *Lavier and Manatschal*, 2006). All the materials used in our modelling experiments have been used in previous studies (*Lavier and Manatschal*, 2006; *Tan et al.*, 2012; *Tan*, 2017). The density and rheological parameters of those materials are listed in Table 1. Note that we use two distinct materials for the upper and lower crust, however, for simplicity purposes, they are both represented in brown in Figures 4 and 5.

5.2 Input Data and Modelling Setup

Large-scale present-day observations from our case studies, presented in sections 3 and 4, are now used as input data of our modelling experiments. These consist of the pre-orogenic rifted margin architecture and the location of the décollement level. Note that in the initial templates of both models (Figures 4a and 5a) a short slab is simulated in the mantle to facilitate subduction initiation in the distal oceanic crust, consistent with *Tan* (2020) and *Auzemery et al.* (2022).

5.2.1 Magma-rich Rifted Margin Model

The modelling setup shown in Figure 4a consists of a pre-reactivated magma-rich rifted margin, characterized by a continental crustal taper thinning out towards a wide oceanic domain. In between the crustal tapper and the ocean, the accommodation space formed by lithospheric stretching is filled in by thinning out syn-kinematic magmatic SDRs which are overlain by post-rift sediments. In contrast with

Table 1 – The density and the rheological parameters of the materials used for the models shown in Figures 4 and 5. The flow law parameters (n, A and E) used in the models are from *Goetze* (1978), *Shelton* (1981), *Ranalli* (1995), *Kirby and Kronenberg* (1987), *Chen and Morgan* (1990).

Material	Flow Law	Density (kg/m^3)	n	A ($MPa^{-n}s^{-1}$)	E(J/mol)	Cohesion, C (Mpa)		Friction angle, φ(°)	
						Initial	Weakened	Initial	Weakened
Continental upper crust	Plagioclase	2800	3.20	$3.30e^{-4}$	$2.38e^{+5}$	40	4	30	15
Continental lower crust	Gabbro	2900	3.05	$1.25e^{-1}$	$3.50e^{+5}$	40	4	30	15
Basaltic SDRs/ Oceanic crust	Basalt	2880	3.05	$1.25e^{-1}$	3.76^{+5}	40	4	30	15
Sediments	Sediments	2600	3.00	$5.00e^{+2}$	2.00^{+5}	4	4	3	3
Mantle	Dry Olivine	3300	3.00	$7.00e^{+4}$	$5.20e^{+5}$	40	4	30	15
Serpentinized mantle	Weak Olivine	3200	3.00	$7.00e^{+4}$	$1.20e^{+5}$	4	4	3	3
Metasediments	Schist	2900	3.00	$7.00e^{+4}$	$3.76e^{+5}$	40	4	30	15

the western Demerara Plateau example, we model a wide oceanic domain following the distal magma-rich rifted margin. This allows us to account for a full mature rift system where an oceanic domain is expected.

As a consequence of the margin architecture setup and the rheological characteristics (i.e. parameters of the viscous flow law) of the material used in the model (see Table 1), the main rheological contrast (MRC) is located at the base of the post-rift sediments (i.e. top magmatic SDRs) (Figure 4b). This is consistent with the western Demerara Plateau observations and implies that the SDRs are coupled with the basement.

5.2.2 Magma-poor Rifted Margin Model

The modelling setup shown in Figure 5a consists of a pre-reactivated magma-poor rifted margin, characterized by a continental crustal taper thinning out towards a wide oceanic domain. In between the crustal tapper and the ocean, the accommodation space is filled in by thinning-out syn-rift sediments that are distally above exhumed mantle and continuously overlain by post-rift sediments. In contrast with the BCB example, we model a wide oceanic domain following the hyper-extended basin floored by exhumed mantle to show the same rift maturity as its end-member magma-rich rifted margin (Figure 4a). Due to the margin architecture setup and the rheological characteristics of the materials used in the model (see Table 1), the main rheological contrast (MRC) is instead located at the base of the syn-rift sediments (Figure 5b). This inherent weakness implies a decoupling between the syn-rift sediments and the basement in agreement with the observations from the BCB example.

6 Modelling Results

We present below how a magma-rich and a magma-poor rifted margins reactivate during early orogenesis through three different model stages presented below (Figures 4 and 5).

In the first model stage, as predetermined in our model setup for both magma-rich and magma-poor rifted margins, subduction of the oceanic crust initiates at the pre-existing slab (Figures 4a and 5b). After 20 Myr of shortening, the oceanic crust is largely subducted below the thick continental crust upper plate and the highest strain rate is focused on the subduction plane (Figures 4c-d and 5c-d). Note that at around 200 km in the x axis of the model, a high strain rate is also observed, leading to crustal thickening (Figures 4c-d and 5c-d). This occurs due to inheritance, characterized by the edge of the post-rift basin.

The second model stage occurs after 30 Myr of shortening, as the inversion of both distal margins, magma-rich and magma-poor, starts (Figures 4e-f and 5e-f). The subduction of oceanic crust is almost achieved for both end-member models, however, note that some oceanic remnants are still preserved in the lower plate (Figures 4e and 5e). At this stage, the localization of the strain-rate of the magma-rich rifted margin (Figure 4e-f) indicates that the deformation propagates upwards into the post-rift sediments, leading to the formation of the very early-stage accretionary wedge (Figure 4e-f). For the reactivated magma-poor rifted margin end-member, the deformation propagates both into and at the base of the post-rift sediments (Figure 5e-f). Note that the latter deformation laterally migrates towards the distal taper of syn-rift sediments (Figure 5e). This shows that at this stage the deformation localizes; (i) at the interface between the sedimentary cover and the exhumed mantle, and (ii) within the post-rift sediments as a fore-thrust leading to the early-stage accretionary wedge formation (Figures 5e-f).

The last model stage displays the deformation after 40 Myr of shortening, showing the end of early orogenesis where both distal rifted margins are reactivated (Figures 4g-h and 5g-h). At this stage the subduction of all oceanic crust is achieved for both magma-rich and magma-poor rifted margins (Figures 4g and 5g). The evolution of the magma-rich rifted margin strain-rate suggests that the deformation is now localized at the interface between the post-rift sediments and the syn-kinematic magmatic SDRs (Figures 4g-h). This

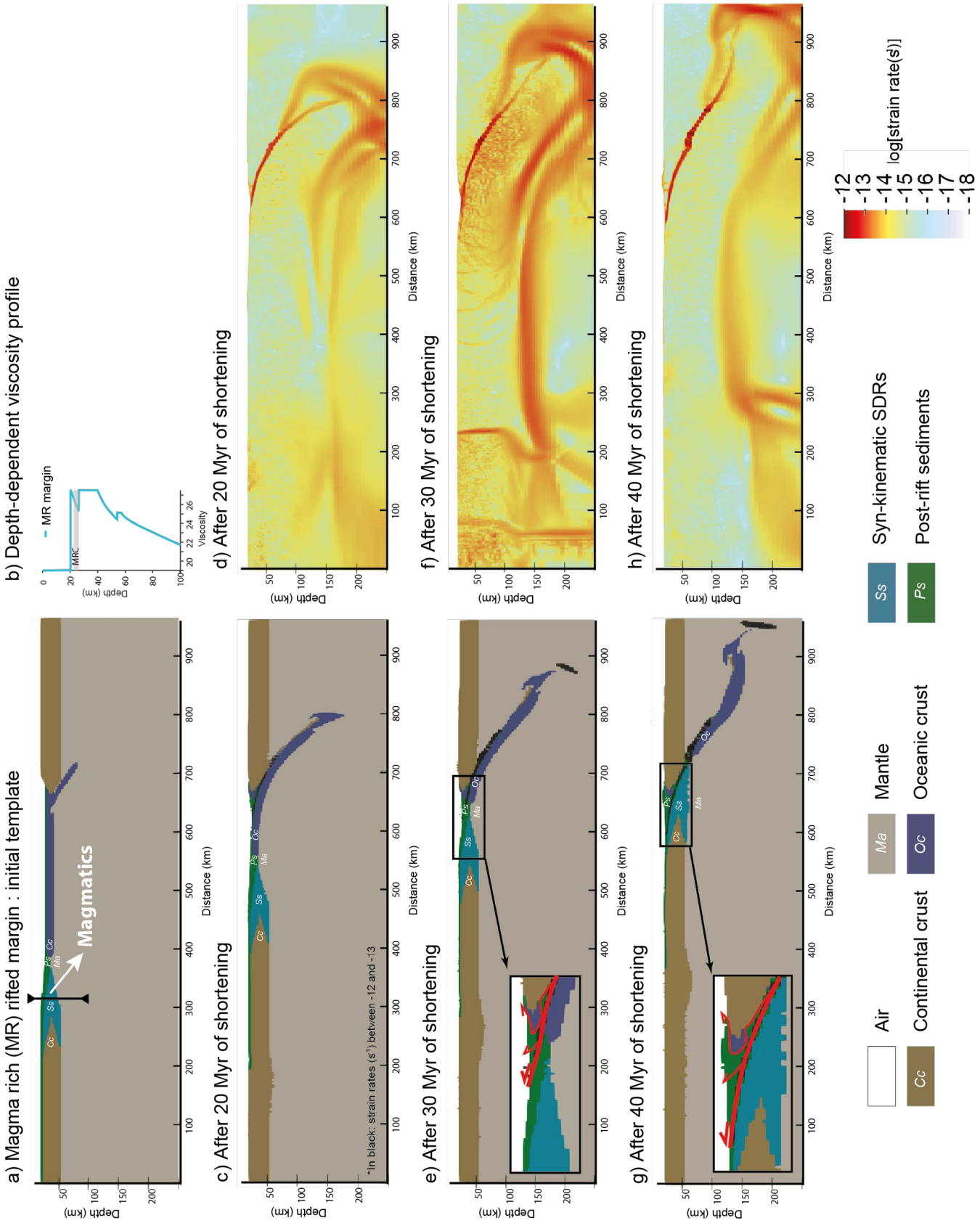

Figure 4 – Results from thermo-mechanical models for a reactivated magma-rich rifted margin. **a-b)** The initial model setup and the depth-dependent viscosity profile respectively. Note that **b)** corresponds to the vertical black line in **a)**. **c-d)** Model stage after 20 Ma of convergence and the associated strain rate deformation respectively. **e-f)** The resulting model and strain rate deformation after 30 Ma of convergence respectively. **g-h)** Last model stage and strain rate deformation respectively characterized by the formation of the early accretionary prism. MRC: Main Rheological Contrast in **b)**.

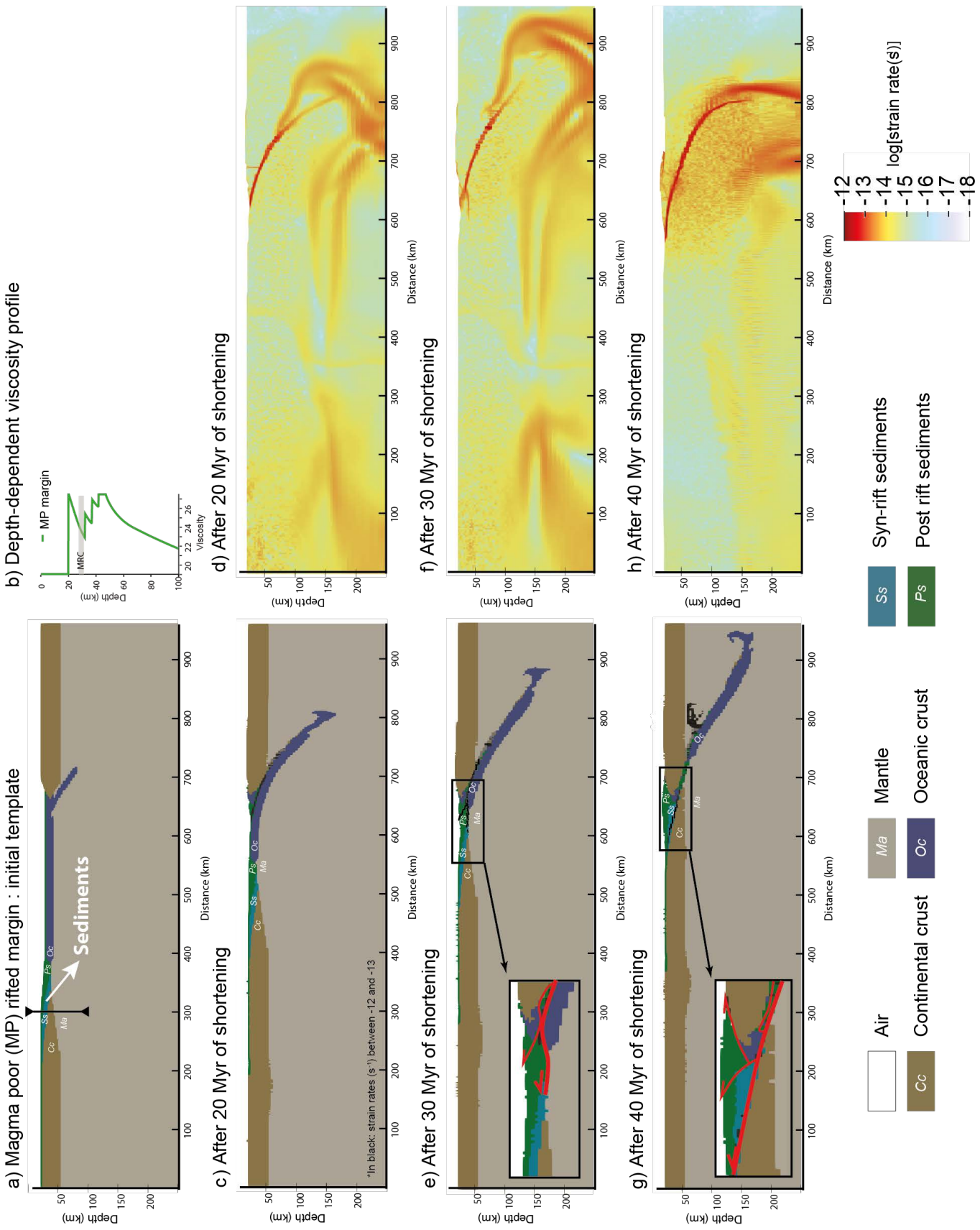

Figure 5 – Same as Figure 4 but showing the evolution of a reactivated magma-poor rifted margin.

indicates that, at the end of early orogenesis resulting from a reactivated magma-rich rifted margin, the main décollement level (MRC in Figure 4b) is at the base of the post-rift sediments controlling the architecture of the early orogenic wedge (Figures 4g-h). Consequently, the syn-kinematic magmatic SDRs and the underlying crustal taper, both corresponding to the lower plate, start to subduct below the upper plate, consisting of thick continental crust, while the post-rift sediments are thrusted and deformed in the accretionary wedge (Figure 4g-h). After 40 Myr of magma-poor rifted margin shortening, the evolution of the strain rate shows that the deformation propagates from the post-rift sediments-mantle interface (model stage after 30 Myr of shortening) to the bottom of the syn-rift sediments (Figures 5g-h). This indicates that, at the end of the early orogenesis stage, the deformation localizes at the interface between the sedimentary cover and the continental crust, giving place to an early orogenic wedge made of both syn- and post-rift sediments above the convergence décollement level (Figures 5g-h). In this setting, the lower plate is made of a crustal taper that starts to subduct below the upper plate consisting of thick continental crust (Figure 5g).

Our modelling results show how distal magma-rich and magma-poor rifted margins reactivate prior to the onset of late orogenesis consisting of crustal thickening (Figures 4 and 5). For the case of a reactivated magma-rich rifted margin, after oceanic crust subduction, the deformation occurs within the post-rift sediments before localizing on top of the syn-kinematic magmatic SDRs (Figures 4c-h). For the case of a reactivated magma-poor rifted margin, after the subduction of the oceanic crust, the deformation initially localizes at the top of the exhumed mantle and below the sedimentary cover. When the exhumed mantle is fully subducted, the deformation localizes at the top of the continental crust and below the sedimentary cover (Figures 5c-h). Note that remnants of oceanic crust can be expected in the early accretionary wedge of both end-member cases (Figures 4g and 5f).

7 Discussion

Our thermo-mechanical modelling results show how magma-rich and magma-poor rifted margins reactivate during early orogenesis, using two natural laboratories as input data. Below we first discuss the learnings of this study for recognizing magma-rich rifted margins within orogens, followed by discussion of the applicability and limitations of our modelling results.

7.1 Insights to Recognize Magma-rich Rifted Margins Within Orogens

The difficulty of recognizing magma-rich rifted margins within orogenic systems worldwide comes from the lack of finding large exposures of syn-kinematic volcanics in early orogenic wedges and/or internal orogenic units. Interestingly, almost half of the worldwide passive margins are magma-rich rifted margins (*Haupert et al.*, 2016, Figure 1). Therefore, it remains unclear why magma-rich rifted margins have not been found within Meso-Cenozoic orogens, while the magma-poor end-member is well-recognized.

Based on this study we provide insights on why magma-rich rifted margins may not be easily identified in orogens by showing the importance of the stratigraphic content of the early orogenic wedge formed during margin inversion (Figures 4, 5, and 6). Only post-rift sediments are preserved when a magma-rich rifted margin is inverted, whereas both syn- and post-rift sediments are sampled in the orogenic wedge as the result of an inverted magma-poor rifted margin (Figures 4g-h and 5g-h). Note that as a result of an inverted magma-poor rifted margin, slices of continental crust and exhumed mantle may also be present as relics of former rift domains (Figure 6c and 6d), however, these are not included in the modelling experiment for simplicity purposes (Figure 5). Reciprocally, we believe that slices of rift-related volcanics below post-rift sediments may also occur in early orogenic wedges, resulting from reactivated magma-rich rifted margins. Our work shows that the different stratigraphic content of early accretionary wedges is controlled by the distinct location of the main convergence décollement level, which localizes below the syn-rift sediments for a distal magma-poor case (Figure 6c and 6d) but is on top of the syn-kinematic magmatics for a distal magma-rich case (Figure 6a and 6b). Additionally, we demonstrate that most of the syn-kinematic magmatic SDRs are expected to be underthrusted beneath the subduction upper plate and therefore are not expected to be found within the accreted material of fold and thrust belts (Figures 4 and 6a-b).

Based on our results, we suggest that the stratigraphic content of an early orogenic wedge is key to determine whether an orogenic system resulted from an inverted magma-rich or magma-poor rifted margin (Figure 6b and 6d). An early orogenic wedge without syn-rift strata formed above a shortened rifted margin may indicate that it derived from a former magma-rich rifted margin (Figure 6a-b). In contrast to that, an early orogenic wedge made of both syn- and post-rift sediments may have resulted from the inversion of a magma-poor rifted margin (Figure 6c-d).

7.2 Applicability and Limitations of our Modelling Results

Our modelling strategy consists of using large-scale present-day observations from our case studies to obtain the input data for our modelling experiments. Below, we explain the similarities and differences between the modelling results and the case study observations which allow us to assess the worldwide applicability and limitations of our approach. These include mainly three parameters: (1) the syn-rift sedi-

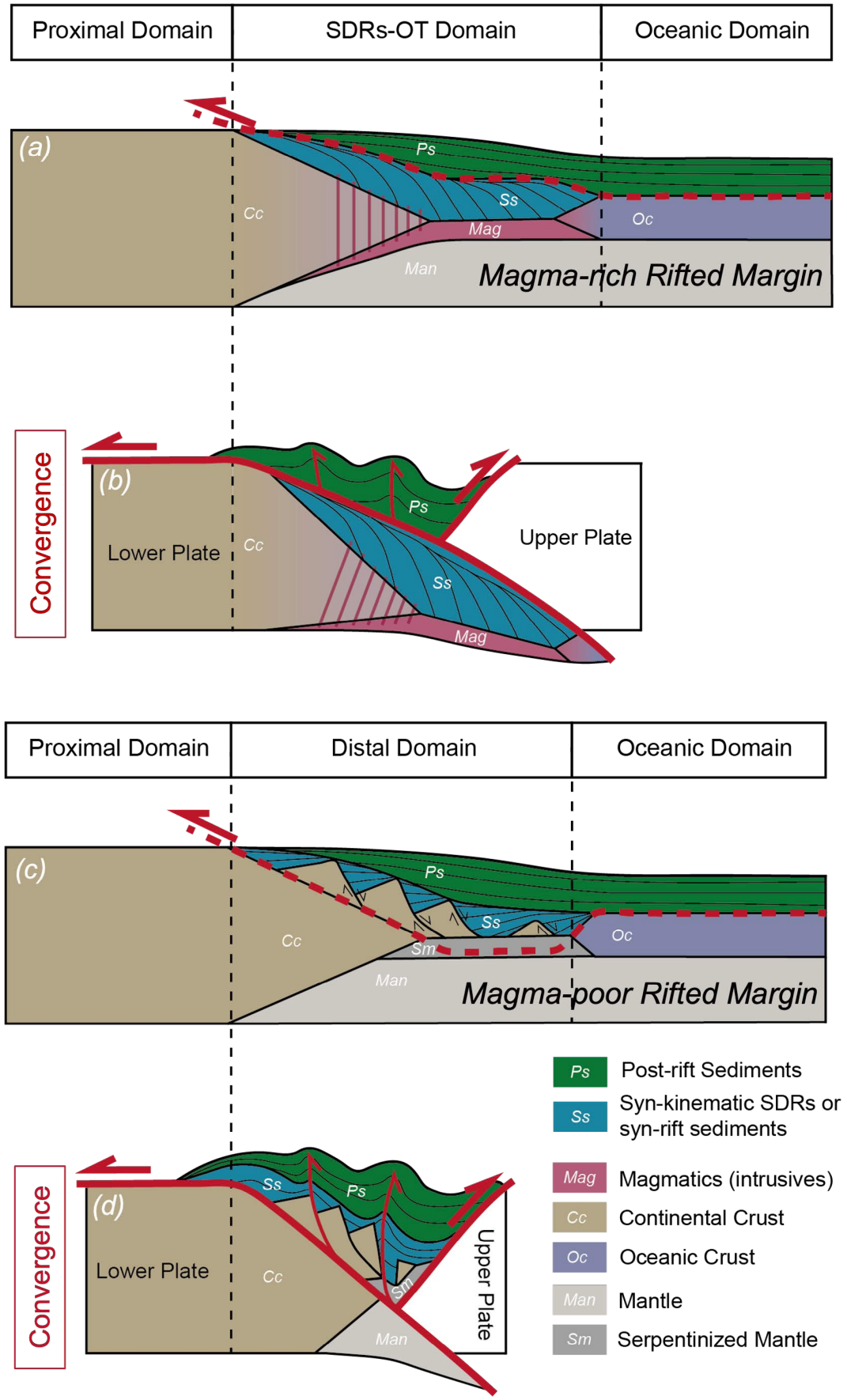

Figure 6 – a-c) Schematic magma-rich and magma-poor rifted margins respectively. The dashed red line corresponds to the future convergence décollement level, located above the SDRs in **a)** and below the syn-rift sediments in **c)**. This structure is active during convergence in **b)** and **d)**. **b-d)** The early accretionary prism resulting from a reactivated magma-rich and a magma-poor rifted margins respectively.

mentation rate, (2) the role of an oceanic domain, and (3) the nature of the upper plate in the resulting architecture of the early orogenic wedge.

7.2.1 The Syn-rift Sedimentation Rate

A low syn-rift sedimentation rate at a magma-poor rifted margin is a parameter that may alter our modelling results. Syn-rift sediment starvation would imply thin syn-rift deposits along rifted margins. Consequently, the reactivation of a magma-poor rifted margin, characterized by a low syn-rift sedimentation rate, would produce an early orogenic wedge made of mostly only post-rift sediments. In contrast, our modelling results show that this stratigraphic content is expected as the result of reactivated magma-rich rifted margins and not of reactivated magma-poor margins. To be able to distinguish between the two end-member reactivated margins in the case of low sedimentation rate, it is therefore also important to investigate the nature of the basement of the margin within slivers in early orogenic thrusts. Slices of serpentinized mantle in addition to syn-rift sediments (as for the BCB example) would indicate a reactivated magma-poor rifted margin, whilst the occurrence of syn-rift volcanics as basal slices below post-rifts sediments would be characteristic of reactivated magma-rich rifted margins.

7.2.2 The Role of an Oceanic Domain

Orogens resulting from margin inversion generally initiate with the closure of wide oceans, followed by a mature subduction, when shortening is driven by slab-pull forces. Consequently, the setup of our modelling experiments consists of pre-reactivated magma-rich and magma-poor rifted margins, including a wide oceanic domain. However, the rift and early orogenic record of mature subduction systems is either pervasively overprinted or destroyed by subduction dynamics (e.g. *Manatschal et al.*, 2022). To overcome this problem, and obtain the record of early orogenesis and the former rift history, it was important that our chosen two case studies had not undergone mature subduction or continent-continent collision (for details see Sections 3 and 4). Shortening in our case studies is controlled by plate convergence. The final modelled stages for both end-member margins (Figures 4g-h and 5g-h) show the same first-order architecture as the observations from our case studies (Figures 2 and 3). This consists of the position of the convergence décollement level, the resulting sedimentary record of the early orogenic wedge, and the nature of the subducted units. These similarities between the models results and the case studies suggest that the presence or not of an oceanic domain does not impact the resulting first-order architecture of the early orogenic wedge. Based on that, we assume that the mechanical behaviour of reactivated rifted margins is controlled by the lithological composition and the thermal state, rather than by the driving mechanism by which the margin inverts. Therefore, we suggest that our results apply not only to our case studies, corresponding to an immature subduction and an early orogenic system, but also to orogenic systems resulting from the closure of wide oceans, following the terminology of *Chenin et al.* (2017).

7.2.3 The Nature of the Upper Plate

Our modelling experiments are focused on the evolution and nature of the lower plate and the resulting sedimentary record of the early accretionary wedge. The nature of the upper plate is not addressed in this study, thus, for simplicity purposes, we model the upper plate as homogenous undifferentiated continental crust (Figures 4 and 5). We believe that considering the upper plate as either continental crust or magmatic-intruded basement would not impact the modelling results from this study. Additionally, regardless of the original nature of the upper plate, subduction dynamics produce melt and magma that can intrude the upper plate. These intrusions would likely affect the deformation of the upper plate during orogenesis, but investigating the role of the upper plate in early orogenesis formation is out of the scope of this study.

7.2.4 Future Perspectives

We studied how two end-member cases of magma-rich and magma-poor rifted margins reactivate during early orogenic processes. We believe, however, that investigating how these end-member margins evolve into late orogenesis would be also important and should be explored in the future. Additionally, gaining insights on how transform margins and transform-overprinted rifted margins reactivate during orogenesis should be the next research step.

8 Conclusions

Numerical modelling results, constrained by observations from two end-member natural laboratories, allow us to better understand the mechanical behaviour of magma-rich and magma-poor rifted margins during early orogenesis. The key conclusions of this study are:

- The location of the main convergence décollement (thin-skinned deformation) during early orogenesis occurs below the syn-rift sediments for distal magma-poor rifted margins, whereas it localizes on top of the syn-kinematic SDRs (volcanics) for distal magma-rich rifted margins.
- Syn-kinematic SDRs (volcanics) are mechanically coupled with their underlying basement, implying that they are likely to be subducted and not accreted during orogenesis. Therefore, they are not expected to be found extensively within mountain belts.
- The accretionary prism stratigraphic content of an orogenic system is key to determine whether the former rift domains were magma-rich or

magma-poor. An accretionary prism made of only post-rift sediments is a key signature of inverted magma-rich rifted margins, whereas the presence of both syn-rift and post-rift sediments rather indicates a former inverted magma-poor margin.

Results from our work show, for the first time, why magma-rich rifted margins are not easily recognized within orogenic systems. This is because only post-rift sediments (and not syn-kinematic volcanics) are expected to be accreted within the early orogenic accretionary wedge as the result of an inverted magma-rich rifted margin.

Acknowledgements

We thank TOTAL for allowing us to use the seismic profile shown in Figure 2. This seismic line is proprietary to ION Geophysical who we thank for allowing us to use and publish it. We would like to thank E. Tan for his help and for giving public access to the geoFLAC code and Luc Lavier for his insights. We also thank reviewers Anouk Beniest and Frank Zwaan for their helpful comments. Tektonika editors, Janine Kavanagh and Adam Forte, are thanked by their comments and smooth handling of the manuscript. Tektonika technical editor, Mohamed Gouiza, is also thanked for copy-editing and type-setting this manuscript.

Author contributions

JGR: Conceptualization, Methodology, Validation, Formal analysis, Investigation, Data Curation, Writing – Original Draft, Visualization. **SJ**: Conceptualization, Methodology, Software, Validation, Formal analysis, Investigation, Data Curation, Writing – Review and Editing, Visualization. **MD**: Conceptualization, Methodology, Validation, Formal Analysis, Investigation, Data Curation, Writing – Review and Editing, Visualization. **RL**: Validation, Writing – Review and Editing, Visualization. **SC**: Validation, Writing – Review and Editing. **EM**: Conceptualization, Methodology, Validation, Formal analysis, Investigation, Resources, Data Curation, Writing – Review and Editing, Visualization, Supervision, Project Administration, Funding Acquisition.

Data availability

Seismic line shown in Figure 2 is proprietary to ION Geophysical. The seismic lines shown in Figure 3 are available on demand using the IGME website (info.igme.es/sigeof/). The geoFLAC code used can be downloaded at https://github.com/tan2/geoflac.

Competing interests

The authors declare no competing interests.

Peer review

This publication was peer-reviewed by Frank Zwaan and Anouk Beniest. The full peer-review report can be found here: https://tektonika.online/index.php/home/article/view/12/8

Copyright notice

References

Auzemery, A., P. Yamato, T. Duretz, E. Willingshofer, L. Matenco, and K. Porkoláb (2022), Influence of magma-poor versus magma-rich passive margins on subduction initiation, *Gondwana Research*, *103*, 172–186, doi: 10.1016/j.gr.2021.11.012.

Barnett-Moore, N., D. R. Müller, S. Williams, J. Skogseid, and M. Seton (2018), A reconstruction of the north atlantic since the earliest jurassic, *Basin Research*, *30*(S1), 160–185, doi: 10.1111/bre.12214.

Basile, C., A. Maillard, M. Patriat, V. Gaullier, L. Loncke, W. Roest, M. Mercier de Lépinay, and F. Pattier (2013), Structure and evolution of the demerara plateau, offshore french guiana: Rifting, tectonic inversion and post-rift tilting at transform–divergent margins intersection, *Tectonophysics*, *591*, 16–29, doi: 10.1016/j.tecto.2012.01.010.

Basile, C., I. Girault, J.-L. Paquette, A. Agranier, L. Loncke, A. Heuret, and E. Poetisi (2020), The jurassic magmatism of the demerara plateau (offshore french guiana) as a remnant of the sierra leone hotspot during the atlantic rifting, *Scientific reports*, *10*(1), 7486, doi: 10.1038/s41598-020-64333-5.

Beltrando, M., G. Manatschal, G. Mohn, G. V. Dal Piaz, A. Vitale Brovarone, and E. Masini (2014), Recognizing remnants of magma-poor rifted margins in high-pressure orogenic belts: The alpine case study, *Earth-Science Reviews*, *131*, 88–115, doi: 10.1016/j.earscirev.2014.01.001.

Bodego, A., E. Iriarte, L. M. Agirrezabala, J. García-Mondéjar, and M. A. López-Horgue (2015), Synextensional mid-cretaceous stratigraphic architecture of the eastern Basque–Cantabrian basin margin (western pyrenees), *Cretaceous Research*, *55*, 229–261, doi: 10.1016/j.cretres.2015.01.006.

Cadenas, P., G. Manatschal, and G. Fernández-Viejo (2020), Unravelling the architecture and evolution of the inverted multi-stage north Iberian-Bay of biscay rift, *Gondwana Research*, *88*, 67–87, doi: 10.1016/j.gr.2020.06.026.

Cámara, P. (2020), Inverted turtle salt anticlines in the eastern Basque-Cantabrian basin, spain, *Marine and Petroleum Geology*, *117*, 104,358, doi: 10.1016/j.marpetgeo.2020.104358.

Chen, Y., and W. J. Morgan (1990), A nonlinear rheology model for mid-ocean ridge axis topography, *Journal of geophysical research*, *95*(B11), 17,583, doi: 10.1029/jb095ib11p17583.

Chenin, P., G. Manatschal, S. Picazo, O. Müntener, G. Karner, C. Johnson, and M. Ulrich (2017), Influence of the architecture of magma-poor hyperextended rifted margins on orogens produced by the closure of narrow versus wide oceans, doi: 10.1130/ges01363.1.

Chenin, P., G. Manatschal, J. Ghienne, and P. Chao (2022), The syn-rift tectono-stratigraphic record of rifted margins (part II): A new model to break through the proximal/distal interpretation frontier, doi: 10.1111/bre.12628.

Chevrot, S., M. Sylvander, J. Diaz, M. Ruiz, and others (2015), The pyrenean architecture as revealed by teleseismic P-to-S converted waves recorded along two dense transects, *Geophysical Journal*.

Choi, E., E. Tan, L. L. Lavier, and V. M. Calo (2013), DynEarthSol2D: An efficient unstructured finite element method to study long-term tectonic deformation, *Journal of Geophysical Research, [Solid Earth]*, *118*(5), 2429–2444, doi: 10.1002/jgrb.50148.

Davis, M., and N. Kusznir (2004), 4. Depth-Dependent lithospheric stretching at rifted continental margins, in *Rheology and Deformation of the Lithosphere at Continental Margins*, pp. 92–137, Columbia University Press.

DeFelipe, I., D. Pedreira, J. A. Pulgar, P. A. Beek, M. Bernet, and R. Pik (2019), Unraveling the mesozoic and cenozoic tectonothermal evolution of the eastern basque-cantabrian zone–western pyrenees by low-temperature thermochronology, *Tectonics*, *38*(9), 3436–3461, doi: 10.1029/2019tc005532.

Ducoux, M., L. Jolivet, J.-P. Callot, C. Aubourg, E. Masini, A. Lahfid, E. Homonnay, F. Cagnard, C. Gumiaux, and T. Baudin (2019), The nappe des marbres unit of the basque-cantabrian basin: The tectono-thermal evolution of a fossil hyperextended rift basin, *Tectonics*, *38*(11), 3881–3915, doi: 10.1029/2018tc005348.

Ducoux, M., L. Jolivet, F. Cagnard, and T. Baudin (2021), Basement-cover decoupling during the inversion of a hyperextended basin: Insights from the eastern pyrenees, *Tectonics*, *40*(5), doi: 10.1029/2020tc006512.

Gillard, M., D. Sauter, J. Tugend, S. Tomasi, M.-E. Epin, and G. Manatschal (2017), Birth of an oceanic spreading center at a magma-poor rift system, *Scientific reports*, *7*(1), 15,072, doi: 10.1038/s41598-017-15522-2.

Goetze, C. (1978), The mechanisms of creep in olivine, *Philosophical transactions of the Royal Society of London. Series A: Mathematical and physical sciences*, *288*(1350), 99–119, doi: 10.1098/rsta.1978.0008.

Gómez-Romeu, J., E. Masini, J. Tugend, M. Ducoux, and N. Kusznir (2019), Role of rift structural inheritance in orogeny highlighted by the western pyrenees case-study, *Tectonophysics*, *766*, 131–150, doi: 10.1016/j.tecto.2019.05.022.

Gómez-Romeu, J., N. Kusznir, M. Ducoux, S. Jammes, P. Ball, S. Calassou, and E. Masini (2022), Formation of SDRs-Ocean transition at magma-rich rifted margins: Significance of a mantle seismic reflector at the western demerara margin, *Tectonophysics*, *845*, 229,624, doi: 10.1016/j.tecto.2022.229624.

Gouiza, M., and D. A. Paton (2019), The role of inherited lithospheric heterogeneities in defining the crustal architecture of rifted margins and the magmatic budget during continental breakup, *Geochemistry, Geophysics, Geosystems*, *20*(4), 1836–1853, doi: 10.1029/2018gc007808.

Gouyet, S., P. Unternehr, and A. Mascle (1994), The french guyana margin and the demerara plateau: Geological history and petroleum plays, in *Hydrocarbon and Petroleum Geology of France*, edited by A. Mascle, pp. 411–422, Springer Berlin Heidelberg, Berlin, Heidelberg, doi: 10.1007/978-3-642-78849-9_29.

Greenroyd, C. J., C. Peirce, M. Rodger, A. B. Watts, and R. W. Hobbs (2007), Crustal structure of the french guiana margin, west equatorial atlantic, *Geophysical Journal International*, *169*(3), 964–987, doi: 10.1111/j.1365-246X.2007.03372.x.

Haupert, I., G. Manatschal, A. Decarlis, and P. Unternehr (2016), Upper-plate magma-poor rifted margins: Stratigraphic architecture and structural evolution, *Marine and Petroleum Geology*, *69*, 241–261, doi: 10.1016/j.marpetgeo.2015.10.020.

Huismans, R. S., and C. Beaumont (2014), Rifted continental margins: The case for depth-dependent extension, doi: 10.1016/j.epsl.2014.09.032.

Hynes, A. (2005), Buoyancy of the oceanic lithosphere and subduction initiation, *International geology review*, *47*(9), 938–951, doi: 10.2747/0020-6814.47.9.938.

Izquierdo-Llavall, E., A. Menant, C. Aubourg, J. Callot, G. Hoareau, P. Camps, E. Péré, and A. Lahfid (2020), Pre-orogenic folds and Syn-Orogenic basement tilts in an inverted hyperextended margin: The northern pyrenees case study, doi: 10.1029/2019tc005719.

Jakob, J., T. B. Andersen, and H. J. Kjøll (2019), A review and reinterpretation of the architecture of the south and South-Central scandinavian Caledonides—A magma-poor to magma-rich transition and the significance of the reactivation of rift inherited structures, *Earth-science reviews*, *192*, 513–528, doi: 10.1016/j.earscirev.2019.01.004.

Jakob, J., H. J. Kjøll, and T. B. Andersen (2022), A fossil magma-rich rifted margin in the scandinavian caledonides, *Continental Rifted Margins 2: Case Examples*, pp. 185–201.

Jammes, S., G. Manatschal, L. Lavier, and E. Masini (2009), Tectonosedimentary evolution related to extreme crustal thinning ahead of a propagating ocean: Example of the western pyrenees, *Tectonics*, *28*(4), doi: 10.1029/2008tc002406.

Jeanniot, L., N. Kusznir, G. Mohn, G. Manatschal, and L. Cowie (2016), Constraining lithosphere deformation modes during continental breakup for the Iberia–Newfoundland conjugate rifted margins, doi: 10.1016/j.tecto.2016.05.006.

Jourdon, A., L. Le Pourhiet, F. Mouthereau, and E. Masini (2019), Role of rift maturity on the architecture and shortening distribution in mountain belts, *Earth and planetary science letters*, *512*, 89–99, doi: 10.1016/j.epsl.2019.01.057.

Kirby, S. H., and A. K. Kronenberg (1987), Rheology of the lithosphere: Selected topics, *Reviews of geophysics*, doi: 10.1029/RG025i006p01219.

Kjøll, H. J., O. Galland, L. Labrousse, and T. B. Andersen (2019), Emplacement mechanisms of a dyke swarm across the brittle-ductile transition and the geodynamic implications for magma-rich margins, *Earth and planetary science letters*, *518*, 223–235, doi: 10.1016/j.epsl.2019.04.016.

Kusznir, N. J., and G. D. Karner (2007), Continental lithospheric thinning and breakup in response to up-

welling divergent mantle flow: application to the woodlark, newfoundland and iberia margins, *Geological Society, London, Special Publications*, *282*(1), 389–419, doi: 10.1144/SP282.16.

Labaume, P., and A. Teixell (2020), Evolution of salt structures of the pyrenean rift (chaînons béarnais, france): From hyper-extension to tectonic inversion, *Tectonophysics*, *785*, 228,451, doi: 10.1016/j.tecto.2020.228451.

Lagabrielle, Y., R. Asti, T. Duretz, C. Clerc, S. Fourcade, A. Teixell, P. Labaume, B. Corre, and N. Saspiturry (2020), A review of cretaceous smooth-slopes extensional basins along the Iberia-Eurasia plate boundary: How pre-rift salt controls the modes of continental rifting and mantle exhumation, *Earth-Science Reviews*, *201*, 103,071, doi: 10.1016/j.earscirev.2019.103071.

Lavier, L. L., and G. Manatschal (2006), A mechanism to thin the continental lithosphere at magma-poor margins, *Nature*, *440*(7082), 324–328, doi: 10.1038/nature04608.

Lavier, L. L., W. R. Buck, and A. N. B. Poliakov (2000), Factors controlling normal fault offset in an ideal brittle layer, *Journal of geophysical research*, *105*(B10), 23,431–23,442, doi: 10.1029/2000jb900108.

Lemoine, M., P. Tricart, and G. Boillot (1987), Ultramafic and gabbroic ocean floor of the ligurian tethys (alps, corsica, apennines): In search of a genetic model, *Geology*, *15*(7), 622–625, doi: 10.1130/0091-7613(1987)15<622:UAGOFO>2.0.CO;2.

Lescoutre, R., and G. Manatschal (2020), Role of rift-inheritance and segmentation for orogenic evolution: example from the Pyrenean-Cantabrian system, *Bulletin de la Société Géologique de France*, *191*(1), doi: 10.1051/bsgf/2020021.

Lescoutre, R., G. Manatschal, and J. A. Muñoz (2021), Nature, origin, and evolution of the Pyrenean-Cantabrian junction, *Tectonics*, *40*(5), doi: 10.1029/2020tc006134.

Loncke, L., M. Mercier de Lépinay, C. Basile, A. Maillard, W. R. Roest, P. De Clarens, M. Patriat, V. Gaullier, F. Klingelhoefer, D. Graindorge, and F. Sapin (2022), Compared structure and evolution of the conjugate demerara and guinea transform marginal plateaus, *Tectonophysics*, *822*, 229,112, doi: 10.1016/j.tecto.2021.229112.

Loparev, A., D. Rouby, D. Chardon, M. Dall'Asta, F. Sapin, F. Bajolet, J. Ye, and F. Paquet (2021), Superimposed rifting at the junction of the central and equatorial atlantic: Formation of the passive margin of the guiana shield, *Tectonics*, *40*(7), doi: 10.1029/2020tc006159.

Lundin, E. R., and A. G. Doré (2011), Hyperextension, serpentinization, and weakening: A new paradigm for rifted margin compressional deformation, *Geology*, *39*(4), 347–350, doi: 10.1130/G31499.1.

Lundin, E. R., A. G. Doré, and T. F. Redfield (2018), Magmatism and extension rates at rifted margins, *Petroleum Geoscience*, *24*(4), 379–392, doi: 10.1144/petgeo2016-158.

Macchiavelli, C., J. Vergés, A. Schettino, M. Fernàndez, E. Turco, E. Casciello, M. Torne, P. P. Pierantoni, and L. Tunini (2017), A new southern north atlantic isochron map: Insights into the drift of the iberian plate since the late cretaceous, *Journal of Geophysical Research, [Solid Earth]*, *122*(12), 9603–9626, doi: 10.1002/2017jb014769.

Manatschal, G. (2004), New models for evolution of magma-poor rifted margins based on a review of data and concepts from west iberia and the alps, *International Journal of Earth Sciences*, *93*(3), 432–466, doi: 10.1007/s00531-004-0394-7.

Manatschal, G., P. Chenin, J.-F. Ghienne, C. Ribes, and E. Masini (2022), The syn-rift tectono-stratigraphic record of rifted margins (part i): Insights from the alpine tethys, *Basin Research*, *34*(1), 457–488, doi: 10.1111/bre.12627.

Martín-Chivelet, J., J. López-Gómez, R. Aguado, C. Arias, J. Arribas, M. E. Arribas, M. Aurell, B. Bádenas, M. I. Benito, T. Bover-Arnal, A. Casas-Sainz, J. M. Castro, F. Coruña, G. A. de Gea, J. J. Fornós, M. Fregenal-Martínez, J. García-Senz, D. Garófano, B. Gelabert, J. Giménez, L. González-Acebrón, J. Guimerà, C. L. Liesa, R. Mas, N. Meléndez, J. M. Molina, J. A. Muñoz, R. Navarrete, M. Nebot, L. M. Nieto, S. Omodeo-Salé, A. Pedrera, C. Peropadre, I. E. Quijada, M. L. Quijano, M. Reolid, A. Robador, J. P. Rodríguez-López, A. Rodríguez-Perea, I. Rosales, P. A. Ruiz-Ortiz, F. Sàbat, R. Salas, A. R. Soria, P. Suarez-Gonzalez, and L. Vilas (2019), The late Jurassic–Early cretaceous rifting, in *The Geology of Iberia: A Geodynamic Approach: Volume 3: The Alpine Cycle*, edited by C. Quesada and J. T. Oliveira, pp. 169–249, Springer International Publishing, Cham, doi: 10.1007/978-3-030-11295-0_5.

Masini, E., G. Manatschal, J. Tugend, G. Mohn, and J.-M. Flament (2014), The tectono-sedimentary evolution of a hyper-extended rift basin: the example of the Arzacq–Mauléon rift system (western pyrenees, SW france), *International Journal of Earth Sciences*, *103*(6), 1569–1596, doi: 10.1007/s00531-014-1023-8.

Mercier de Lépinay, M., L. Loncke, C. Basile, W. R. Roest, M. Patriat, A. Maillard, and P. De Clarens (2016), Transform continental margins – part 2: A worldwide review, *Tectonophysics*, *693*, 96–115, doi: 10.1016/j.tecto.2016.05.038.

Miró, J., G. Manatschal, P. Cadenas, and J. A. Muñoz (2021), Reactivation of a hyperextended rift system: The Basque–Cantabrian pyrenees case, *Basin Research*, *33*(6), 3077–3101, doi: 10.1111/bre.12595.

Mohn, G., G. Manatschal, O. Müntener, M. Beltrando, and E. Masini (2010), Unravelling the interaction between tectonic and sedimentary processes during lithospheric thinning in the alpine tethys margins, *International Journal of Earth Sciences*, *99*(1), 75–101, doi: 10.1007/s00531-010-0566-6.

Mohn, G., G. Manatschal, M. Beltrando, E. Masini, and N. Kusznir (2012), Necking of continental crust in magma-poor rifted margins: Evidence from the fossil alpine tethys margins, *Tectonics*, *31*(1), TC1012, doi: 10.1029/2011TC002961.

Museur, T., D. Graindorge, F. Klingelhoefer, W. R. Roest, C. Basile, L. Loncke, and F. Sapin (2021), Deep structure of the demerara plateau: From a volcanic margin to a transform marginal plateau, *Tectonophysics*, *803*, 228,645, doi: 10.1016/j.tecto.2020.228645.

Nemčok, M., S. Rybár, P. Ekkertová, J. Kotulová, S. A. Hermeston, and D. Jones (2016), Transform-margin model of hydrocarbon migration: the Guyana–Suriname case study, *Geological Society, London, Special Publications*, *431*(1), 199–217, doi: 10.1144/SP431.6.

Nirrengarten, M., G. Manatschal, J. Tugend, N. J. Kusznir, and D. Sauter (2017), Nature and origin of the j-magnetic anomaly offshore Iberia-Newfoundland: implications for plate reconstructions, *Terra nova*, *29*(1), 20–28, doi: 10.1111/ter.12240.

Norcliffe, J. R., D. A. Paton, E. J. Mortimer, A. M. McCaig, H. Nicholls, K. Rodriguez, N. Hodgson, and D. Van

Der Spuy (2018), Laterally confined volcanic successions (LCVS); recording rift-jumps during the formation of magma-rich margins, *Earth and planetary science letters*, *504*, 53–63, doi: 10.1016/j.epsl.2018.09.033.

Olivet, J. L. (1996), La cinématique de la plaque ibérique, *Bulletin des centres de recherches exploration*.

Osmundsen, P. T., and T. F. Redfield (2011), Crustal taper and topography at passive continental margins, *Terra nova*, *23*(6), 349–361, doi: 10.1111/j.1365-3121.2011.01014.x.

Pedreira, D., J. A. Pulgar, J. Gallart, and M. Torné (2007), Three-dimensional gravity and magnetic modeling of crustal indentation and wedging in the western Pyrenees-Cantabrian mountains, *Journal of geophysical research*, *112*(B12), doi: 10.1029/2007jb005021.

Pedrera, A., J. García-Senz, C. Ayala, A. Ruiz-Constán, L. R. Rodríguez-Fernández, A. Robador, and L. González Menéndez (2017), Reconstruction of the exhumed mantle across the north iberian margin by crustal-scale 3-D gravity inversion and geological cross section, *Tectonics*, *36*(12), 3155–3177, doi: 10.1002/2017tc004716.

Péron-Pinvidic, G., and G. Manatschal (2009), The final rifting evolution at deep magma-poor passive margins from Iberia-Newfoundland: a new point of view, *International Journal of Earth Sciences*, *98*(7), 1581–1597, doi: 10.1007/s00531-008-0337-9.

Péron-Pinvidic, G., G. Manatschal, S. M. Dean, and T. A. Minshull (2008), Compressional structures on the west iberia rifted margin: controls on their distribution, *Geological Society, London, Special Publications*, *306*(1), 169–183, doi: 10.1144/SP306.8.

Poliakov, A. N. B., Y. Podladchikov, and C. Talbot (1993), Initiation of salt diapirs with frictional overburdens: numerical experiments, *Tectonophysics*, *228*(3), 199–210, doi: 10.1016/0040-1951(93)90341-G.

Ranalli, G. (1995), *Rheology of the Earth*, Springer Science & Business Media.

Ranero, C. R., and M. Pérez-Gussinyé (2010), Sequential faulting explains the asymmetry and extension discrepancy of conjugate margins, *Nature*, *468*(7321), 294–299, doi: 10.1038/nature09520.

Reuber, K. R., J. Pindell, and B. W. Horn (2016), Demerara rise, offshore suriname: Magma-rich segment of the central atlantic ocean, and conjugate to the bahamas hot spot, *Interpretation*, *4*(2), T141–T155, doi: 10.1190/INT-2014-0246.1.

Roca, E., J. A. Muñoz, O. Ferrer, and N. Ellouz (2011), The role of the bay of biscay mesozoic extensional structure in the configuration of the pyrenean orogen: Constraints from the MARCONI deep seismic reflection survey, *Tectonics*, *30*(2), doi: 10.1029/2010tc002735.

Roest, W. R., and S. P. Srivastava (1991), Kinematics of the plate boundaries between eurasia, iberia, and africa in the north atlantic from the late cretaceous to the present, *Geology*, *19*(6), 613–616, doi: 10.1130/0091-7613(1991)019<0613:KOTPBB>2.3.CO;2.

Saspiturry, N., A. Lahfid, T. Baudin, L. Guillou-Frottier, P. Razin, B. Issautier, B. Le Bayon, O. Serrano, Y. Lagabrielle, and B. Corre (2020), Paleogeothermal gradients across an inverted hyperextended rift system: Example of the mauléon fossil rift (western pyrenees), *Tectonics*, *39*(10), doi: 10.1029/2020tc006206.

Shelton, G. (1981), Experimental flow laws for crustal rocks, *Eos, Transactions, American Geophysical Union*, *62*, 396.

Shillington, D. J., C. L. Scott, T. A. Minshull, R. A. Edwards, P. J. Brown, and N. White (2009), Abrupt transition from magma-starved to magma-rich rifting in the eastern black sea, *Geology*, *37*(1), 7–10, doi: 10.1130/G25302A.1.

Sibuet, J.-C., S. P. Srivastava, and W. Spakman (2004), Pyrenean orogeny and plate kinematics, *Journal of geophysical research*, *109*(B8), doi: 10.1029/2003jb002514.

Srivastava, S. P., W. R. Roest, L. C. Kovacs, G. Oakey, S. Lévesque, J. Verhoef, and R. Macnab (1990), Motion of iberia since the late jurassic: Results from detailed aeromagnetic measurements in the newfoundland basin, *Tectonophysics*, *184*(3), 229–260, doi: 10.1016/0040-1951(90)90442-B.

Stab, M., N. Bellahsen, R. Pik, X. Quidelleur, D. Ayalew, and S. Leroy (2016), Modes of rifting in magma-rich settings: Tectono-magmatic evolution of central afar, *Tectonics*, *35*(1), 2–38, doi: 10.1002/2015tc003893.

Stica, J. M., P. V. Zalán, and A. L. Ferrari (2014), The evolution of rifting on the volcanic margin of the pelotas basin and the contextualization of the Paraná–Etendeka LIP in the separation of gondwana in the south atlantic, *Marine and Petroleum Geology*, *50*, 1–21, doi: 10.1016/j.marpetgeo.2013.10.015.

Sutra, E., and G. Manatschal (2012), How does the continental crust thin in a hyperextended rifted margin? insights from the iberia margin, *Geology*, *40*(2), 139–142, doi: 10.1130/G32786.1.

Sutra, E., G. Manatschal, G. Mohn, and P. Unternehr (2013), Quantification and restoration of extensional deformation along the western iberia and newfoundland rifted margins, *Geochemistry, Geophysics, Geosystems*, *14*(8), 2575–2597, doi: 10.1002/ggge.20135.

Svartman Dias, A. E., L. L. Lavier, and N. W. Hayman (2015), Conjugate rifted margins width and asymmetry: The interplay between lithospheric strength and thermomechanical processes, *Journal of Geophysical Research, [Solid Earth]*, *120*(12), 8672–8700, doi: 10.1002/2015jb012074.

Tan, E. (2017), Mantle wedge serpentinization effects on slab dips, *TAO: Terrestrial, Atmospheric and Oceanic Sciences*, *28*(3), 2.

Tan, E. (2020), Subduction of transitional crust at the manila trench and its geophysical implications, *Journal of Asian Earth Sciences*, *187*, 104,100, doi: 10.1016/j.jseaes.2019.104100.

Tan, E., L. L. Lavier, H. J. A. Van Avendonk, and A. Heuret (2012), The role of frictional strength on plate coupling at the subduction interface, *Geochemistry, Geophysics, Geosystems*, *13*(10), Q10,006, doi: 10.1029/2012GC004214.

Tavani, S., C. Bertok, P. Granado, F. Piana, R. Salas, B. Vigna, and J. A. Muñoz (2018), The Iberia-Eurasia plate boundary east of the pyrenees, *Earth-Science Reviews*, *187*, 314–337, doi: 10.1016/j.earscirev.2018.10.008.

Tavani, S., P. Granado, A. Corradetti, G. Camanni, G. Vignaroli, G. Manatschal, S. Mazzoli, J. A. Muñoz, and M. Parente (2021), Rift inheritance controls the switch from thin- to thick-skinned thrusting and basal décollement relocalization at the subduction-to-collision transition, *GSA Bulletin*, *133*(9-10), 2157–2170, doi: 10.1130/B35800.1.

Tomasi, S., N. Kusznir, G. Manatschal, and F. Despinois (2021), The challenge in restoring magma-rich rifted margins: The example of the Mozambique-Antarctica conjugate margins, *Gondwana Research*, *95*, 29–44, doi:

10.1016/j.gr.2021.03.009.

Trude, J., B. Kilsdonk, T. Grow, and B. Ott (2023), The structure and tectonics of the guyana basin, *Geological Society, London, Special Publications*, *524*(1), SP524–2021–117, doi: 10.1144/SP524-2021-117.

Tugend, J., G. Manatschal, N. J. Kusznir, E. Masini, G. Mohn, and I. Thinon (2014), Formation and deformation of hyperextended rift systems: Insights from rift domain mapping in the bay of Biscay-Pyrenees, *Tectonics*, *33*(7), 1239–1276, doi: 10.1002/2014tc003529.

Tugend, J., M. Gillard, G. Manatschal, M. Nirrengarten, C. Harkin, M.-E. Epin, D. Sauter, J. Autin, N. Kusznir, and K. McDermott (2020), Reappraisal of the magma-rich versus magma-poor rifted margin archetypes, *Geological Society, London, Special Publications*, *476*(1), 23–47, doi: 10.1144/SP476.9.

Verhoef, J., and S. P. Srivastava (1989), Correlation of Sedimentary Basins Across the North Atlantic as Obtained from Gravity and Magnetic Data, and Its Relation to the Early Evolution of the North Atlantic, in *Extensional Tectonics and Stratigraphy of the North Atlantic Margins*, American Association of Petroleum Geologists, doi: 10.1306/M46497C9.

Vissers, R. L. M., and P. T. Meijer (2012), Iberian plate kinematics and alpine collision in the pyrenees, *Earth-Science Reviews*, *114*(1), 61–83, doi: 10.1016/j.earscirev.2012.05.001.

Vissers, R. L. M., D. J. J. van Hinsbergen, D. G. van der Meer, and W. Spakman (2016), Cretaceous slab break-off in the pyrenees: Iberian plate kinematics in paleomagnetic and mantle reference frames, *Gondwana Research*, *34*, 49–59, doi: 10.1016/j.gr.2016.03.006.

Watremez, L., S. Leroy, E. d'Acremont, V. Roche, M. Evain, A. Leprêtre, F. Verrier, D. Aslanian, N. Dias, A. Afilhado, P. Schnürle, R. Castilla, F. Despinois, and M. Moulin (2021), The limpopo magma-rich transform margin, south mozambique: 1. insights from deep-structure seismic imaging, *Tectonics*, *40*(12), doi: 10.1029/2021tc006915.

Whitmarsh, R. B., P. R. Miles, and A. Mauffret (1990), The ocean-continent boundary off the western continental margin of Iberia—I. crustal structure at 40°30'n, *Geophysical Journal International*, *103*(2), 509–531, doi: 10.1111/j.1365-246X.1990.tb01788.x.

Zhou, X., Z.-H. Li, T. V. Gerya, R. J. Stern, Z. Xu, and J. Zhang (2018), Subduction initiation dynamics along a transform fault control trench curvature and ophiolite ages, *Geology*, *46*(7), 607–610, doi: 10.1130/G40154.1.